Journal of Solid State Chemistry 181 (2008) 3278–3282

Contents lists available at ScienceDirect

Journal of Solid State Chemistry

journal homepage: www.elsevier.com/locate/jssc

Enhanced thermoelectric properties of bismuth sulfide polycrystals prepared by mechanical alloying and spark plasma sintering

Li-Dong Zhao [a,b], Bo-Ping Zhang [a,*], Wei-Shu Liu [a,b], Hai-Long Zhang [a], Jing-Feng Li [b,**]

[a] School of Materials Science and Engineering, University of Science and Technology Beijing, Beijing 100083, China
[b] State Key Laboratory of New Ceramics and Fine Processing, Department of Materials Science and Engineering, Tsinghua University, Beijing 100084, China

ARTICLE INFO

Article history:
Received 12 June 2008
Received in revised form
20 July 2008
Accepted 12 August 2008
Available online 27 August 2008

Keywords:
Bismuth sulfides
Mechanical alloying
Spark plasma sintering
Thermoelectric

ABSTRACT

Bismuth sulfide powders were synthesized by mechanical alloying (MA) and then consolidated by spark plasma sintering (SPS) technique. In order to improve the electrical transport properties of bismuth sulfides, the carrier concentration was optimized by modifying chemical composition of sulfur through producing sulfur vacancies, and the carrier mobility was enhanced by a two-step SPS as a hot-forging process through increasing grain orientation. The electrical resistivity of bismuth sulfides was reduced to 10^{-4} from $10^{-2}\,\Omega$ m by optimizing sulfur content, and further lowered by hot-forging, whereby the power factor was significantly increased from 91 to 254 $\mu W/mK^2$. The hot-forged $Bi_2S_{2.90}$ sample showed the highest $ZT = 0.11$ (at 523 K), which is higher than the reported value. The present work revealed that bismuth sulfide compounds as a promising candidate of thermoelectric materials can be synthesized by a simple process.

1. Introduction

Thermoelectric (TE) power generators and refrigerators are solid-state devices without moving parts. They are silent, reliable and scalable, making them ideal for small, distributed power generation [1]. The efficiency of TE devices is determined by the dimensionless figure of merit (ZT), defined as $ZT = (\alpha^2/\rho k)T$, where α, ρ, k, and T are the Seebeck coefficient, electrical resistivity, thermal conductivity, and absolute temperature, respectively. The compounds A_2B_3 (where $A = $ Bi, Sb, Pb and $B = $ S, Se, Te) are considered to be most promising for TE applications [2]. Bi–Te-based [3] and Pb–Te-based [4,5] compounds show the best TE properties at room and middle temperatures, respectively. Although telluride-based materials usually exhibit good TE properties and hold dominant market shares in TE materials, it is necessary to develop alternative materials to replace the rare and toxic tellurium. Bismuth sulfide (Bi_2S_3) belongs to the A_2B_3 family, but little attention has been paid to Bi_2S_3 in TE development because of its high electrical resistivity due to a 1.30 eV direct band gap at room temperature [6]. It is quite encouraging that the electrical resistivity of Bi_2S_3 can be reduced by 2–3 orders of magnitude through introducing sulfur vacancies in the lattice [7]. Surprisingly, the low thermal conductivity of the sulfur-deficient Bi_2S_3 could be realized by enhancing phonon scattering on the sulfur vacancies, where the large Seebeck coefficient was maintained at same time as suggested by Chen [8]. Enhanced high electrical transport properties were achieved in the one-dismensional Bi_2S_3 films by increasing carrier mobility using its natural anisotropic [9]. Although the polycrystals of TE materials own the better mechanical properties and lower thermal conductivity, little attention has been paid to polycrystalline Bi_2S_3 materials until now probably because of their high electrical resistivity. It was found that fine-grained and textured Bi_2Te_3 TE materials which are fabricated by SPS possess high performance [10]. Therefore, we expect to enhance the electrical transport properties especially power factor by tailoring stoichiometric ratio of bismuth to sulfur and controlling grain orientation, meanwhile, to reduce the thermal conductivity by refining grain size.

In the present study, Bi_2S_3 polycrstals with substoichiometry and oriented fine grains were successfully fabricated by mechanical alloying (MA) and SPS technique. The microstructure and TE properties were investigated with special emphases on the effects of sulfur content and orientation degree. The highest ZT value known presently achieved 0.11 at 523 K in the Bi_2S_3's family.

2. Experimental procedure

Commercial high-purity powders of 99.999% Bi and 99.9% S under the same 100 mesh were used as raw materials. The

* Corresponding author.
** Also for correspondence. Fax: +8610 62771160.
E-mail addresses: bpzhang@mater.ustb.edu.cn (B.-P. Zhang), jingfeng@mail.tsinghua.edu.cn (J.-F. Li).

0022-4596/$ - see front matter © 2008 Published by Elsevier Inc.
doi:10.1016/j.jssc.2008.08.022

powders with the chemical composition of Bi_2S_{3-x} ($x = 0$, 0.05, 0.10, 0.15) were MAed at 350 rpm for 15 h in a purified argon atmosphere using a planetary ball mill (QM-1SP2, Nanjing University, China). Stainless steel vessel and balls were used, and the weight ratio of ball to powder was kept at 20:1. The MAed powders were firstly SPSed at 673 K for 5 min in a Φ15 mm graphite mould under the axial compressive stress of 50 MPa in vacuum using a SPS system (Sumimoto SPS1050, Japan), resulting in a disk-shaped bulk of Φ15 mm × 6 mm. The SPSed Φ15 mm × 6 mm bulks were then charged to a Φ20 mm graphite mould and were SPSed again at 723 K for 5 min, acting as a hot-forging process. The other conditions were the same as the first SPS processing. Finally, disk-shaped samples with dimensions of Φ20 mm × 4.5 mm were obtained.

Phase structure was analyzed by X-ray diffraction (XRD, Cu$K\alpha$, Bruker D8, Germany). The morphologies of powder and fractographs of bulks were observed by scanning electron microscopy (SEM, JSM-6460, Japan). The TE properties were evaluated along the sample section perpendicular to the pressing direction of SPS. The Seebeck coefficient and electrical resistivity were measured at 323–573 K in a helium atmosphere using a Seebeck coefficient/electric resistance measuring system (ZEM-2, Ulvac-Riko, Japan). The thermal diffusivity coefficient (D) was measured using the laser flash method (NETZSCH, LFA427, Germany). The specific heat (C_p) was measured using a thermal analyzing apparatus (Dupont 1090B, USA). The density (d) of the sample was measured by the Archimedes method. The thermal conductivity (k) was calculated from the product of thermal diffusivity, specific heat (C_p) and density, $k = D\ C_p\ d$. The Hall coefficients, R_H, of the samples were measured at room temperature using a physical properties measurement system (PPMS-9T, Quantum Design Inc., USA), and a magnetic field of 2 T and electrical current of 30 mA were applied. The carrier concentration (n) was calculated by $n = 1/eR_H$, where e is the electronic charge. The carrier mobility (μ) was calculated by $\mu = R_H/\rho$, where ρ is the electrical resistivity.

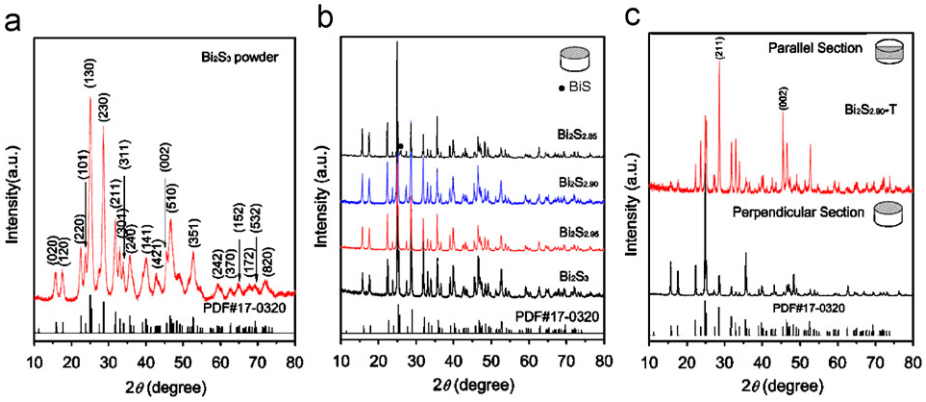

Fig. 1. XRD patterns of the MAed Bi_2S_3 powders (a), the SPSed Bi_2S_{3-x} ($x = 0.0$, 0.05, 0.10, 0.15) bulks (b), and the hot-forged $Bi_2S_{2.90}$ bulks (c) in perpendicular and parallel to the pressing direction.

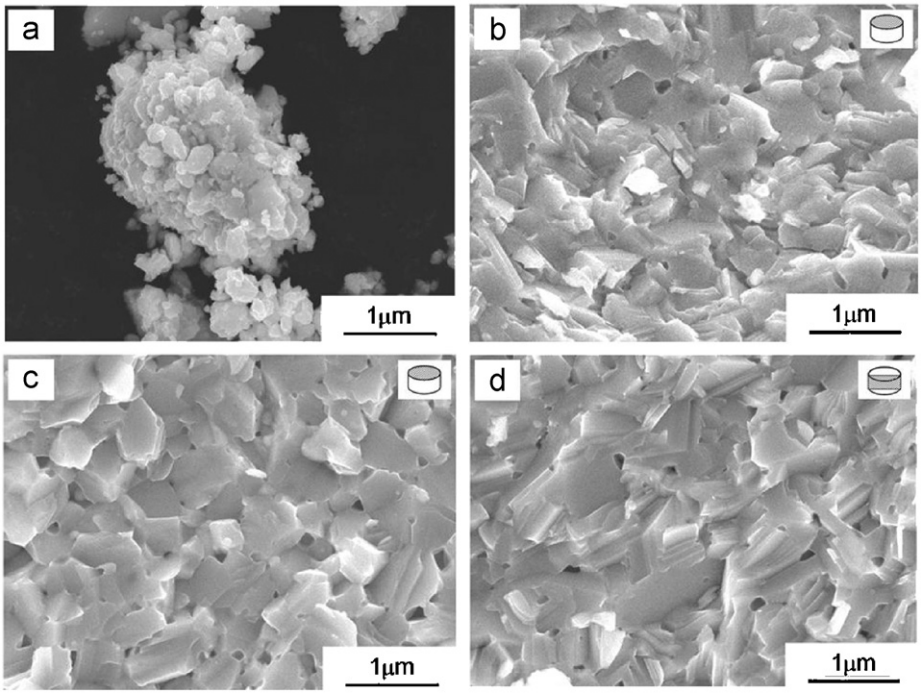

Fig. 2. SEM micrographs of the MAed Bi_2S_3 powders (a) as well as the fractured surfaces of $Bi_2S_{2.90}$ bulk before (b) and after (c, d) hot forging, in which the fractured surfaces of the later two hot-forged samples are perpendicular (c) and parallel (d) to the pressing direction, respectively.

3. Results and discussion

Fig. 1 shows XRD patterns of the Bi_2S_3 powders and bulks. As shown in Fig. 1(a), the XRD patterns of the MAed Bi_2S_3 powder verify that the powder is in a single phase with a well-matched patterns to the binary Bi_2S_3 (PDF#17-0320), which indicates that Bi_2S_3 powders were successfully synthesized by the MA method. Compared with other synthesis methods such as Bridgman [6] and melting in vacuum-sealed tube [8], MA is an effective method to synthesize the compounds composed of volatile elements with low melting point [11]. Fig. 1(b) shows the XRD patterns of the Bi_2S_3 bulks with different sulfur contents which are expressed as Bi_2S_{3-x} ($x = 0.0$, 0.05, 0.10, 0.15). The Bi_2S_3 bulks obtained from the section perpendicular to the pressing direction show the similar XRD patterns to that of MAed Bi_2S_3 powder regardless of the sulfur content. However, the deficient sulfur in the $Bi_2S_{2.85}$ sample results in the appearance of impurity phases BiS. Fig. 1(c) shows the XRD patterns of $Bi_2S_{2.90}$ bulks after hot-forging, it should be noted that the XRD patterns of hot-forged $Bi_2S_{2.90}$ bulks in perpendicular and parallel to the pressing direction shows the different intensities in several characteristic peaks due to the anisotropic chemical-bonds of the Bi_2S_3 crystals. Covalent bonds are directed along the *c*-axis, while along the *a* and *b* directions, bonding is made by weak ionic and van der Waals forces [12]. Therefore, Bi_2S_3 is featured with a layer structure and the crystal is easily cleaved parallel to the *c*-axis. The grains cleaved and compactly stacked up along the pressing direction by hot-forging. As a result, the cleaved planes along the *c*-axis are perpendicular to the pressing direction. Therefore, the hot-forged $Bi_2S_{2.90}$ bulks in the sections parallel to the pressing direction show much stronger diffraction intensities at (0 0 2) and (2 1 1) planes, in which the angle between [2 1 1] and *c*-axis is 70.53°. The XRD results indicate that $Bi_2S_{2.90}$ bulks with grain orientation texture (shortly named $Bi_2S_{2.90}$-T) was obtained by hot-forging deformation through the extra space in the larger mould.

Fig. 2 shows the SEM micrographs of the MAed Bi_2S_3 powders and the fractured surfaces of $Bi_2S_{2.90}$ bulks. As shown in Fig. 2(a), the MA process produced very fine Bi_2S_3 powders with particles sizes in several hundred nanometers. The grains of $Bi_2S_{2.90}$ sample SPSed at 673 K were randomly arranged and experienced slight growth compared with Bi_2S_3 powders, as shown in Fig. 2(b). The Bi_2S_{3-x} ($x = 0.0$, 0.05, 0.15) samples SPSed at 673 K showed the similar microstructure to that of $Bi_2S_{2.90}$ ($x = 0.1$). The grains of hot-forged $Bi_2S_{2.90}$ sample in both sections perpendicular and parallel to the pressing direction show the flat and lamellar morphologies, respectively. Because the grains cleave easily along the *c*-axis and tend to be rearranged under an applied pressure, the cleavage planes are inclined to perpendicular to the pressing direction. The SEM microstructures for Bi_2S_3's are consistent well with the XRD observations.

Fig. 3 shows the temperature dependence of electrical transport properties for Bi_2S_3's. Fig. 3(a) is the variations of Seebeck coefficient as a function of measuring temperature. The negative values of Seebeck coefficient indicate that all the samples are *n*-type and the major carrier is electron. The magnitude of Seebeck coefficient for the Bi_2S_3 sample show the highest values of about $-500\,\mu V/K$ at 323–573 K measuring temperatures as shown in inset of Fig. 3(a). The Seebeck coefficients for Bi_2S_{3-x} ($x>0$) samples are ranged from -300 to $-400\,\mu V/K$, which are 20% lower than that of Bi_2S_3 sample. According to the Ioffe theory, the Seebeck coefficient is inversely proportional to the carrier concentration [13]. Therefore, the decreased Seebeck coefficient for Bi_2S_{3-x} ($x>0$) samples could be ascribed to the increase in carrier concentration as listed in Table 1, which was measured at room temperature. The carrier concentration increases by two orders of magnitude from $10^{16}/cm^3$ for Bi_2S_3 to $10^{18}/cm^3$ for

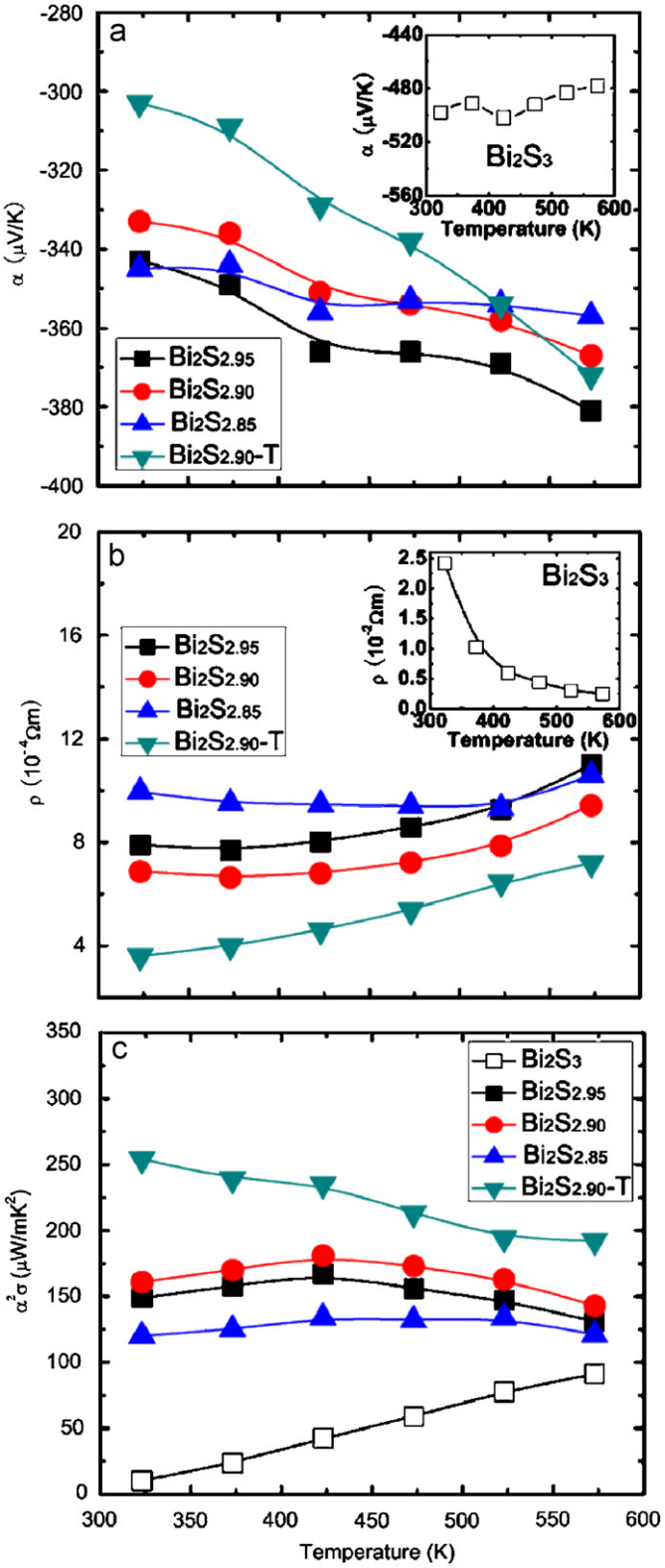

Fig. 3. Temperature dependence of electrical resistivity (a), Seebeck coefficient (b), and power factor (c) for Bi_2S_3's.

Bi_2S_{3-x} ($x>0$) by modifying the ratio of bismuth and sulfur from stoichiometric to substoichiometric one. Reducing a sulfur atom in Bi_2S_3's should generate sulfur vacancies $V_S^{\bullet\bullet}$, resulting in increasing electrons. This process can be described by the

Table 1
Density, carrier concentration, and mobility for bismuth sulfides

Samples	Measured density (g/cm^3)	Relative density[a] (%)	Carrier concentration, n (10^{18}/cm^3)	Carrier mobility, μ (cm^2/V s)
Bi_2S_3	6.29	92.4	0.05	246
$Bi_2S_{2.95}$	6.28	92.2	2.98	265
$Bi_2S_{2.90}$	6.30	92.6	4.17	218
$Bi_2S_{2.85}$	6.31	92.7	2.60	241
$Bi_2S_{2.90}$-T	6.26	91.9	3.47	500

[a] With regard to the theoretical density of 6.81 g/cm^3 [14].

following equation:

$$Bi_2S_{3-x} = Bi_2S_3 - xS + xV_S^{\bullet\bullet} + 2xe' \quad (1)$$

where e' is the produced electron, which can cause an increase in carrier (electron) concentration for n-type materials. The increased carrier concentration by reducing the sulfur content will produce the decrease in the Seebeck coefficient.

Fig. 3(b) shows the electrical resistivity as a function of measuring temperature for the Bi_2S_3's. The electrical resistivities for Bi_2S_3 sample decrease with increasing temperature, which shows a semiconductor conducting behavior, as shown in the inset of Fig. 3(b). However, the electrical resistivities for all the Bi_2S_{3-x} ($x>0$) samples increase with increasing temperature, showing a metallic conducting behavior. The electrical resistivity of Bi_2S_{3-x} ($x>0$) samples is two orders of magnitude $10^{-4}\,\Omega$ m lower than $10^{-2}\,\Omega$ m of Bi_2S_3 sample in the whole measuring temperature range from 323 to 573 K. The effect of sample density could be excluded since the relative densities for all the samples are close to each other as listed in Table 1. It is well known that the electrical resistivity determined competitively by carrier concentration and mobility as described by the relationship, $\rho = 1/ne\mu$, where ρ, μ and e are the electrical resistivity, the carrier mobility, and the electron charge, respectively. The carrier concentration increases with decreasing sulfur content due to the formation of sulfur vacancies, whereby the electrical resistivities for the Bi_2S_{3-x} ($x>0$) samples decrease with reducing sulfur content. However, the electrical resistivity was found to increases as the sulfur content further decreases to $x = 2.85$, which ascribes to the appearance of impurity phase (BiS) in $Bi_2S_{2.85}$ sample. As shown in Fig. 3(b), the $Bi_2S_{2.90}$ sample shows the lowest electrical resistivity among the Bi_2S_{3-x} ($x>0$) samples, and that further decreases after hot-forging. The carrier mobility of the $Bi_2S_{2.90}$ sample (in Table 1) is found to increase from 218 cm^2/V s to 500 cm^2/V s by hot-forging. The increased carrier mobility contributes to the decrease in electrical resistivity. The XRD and SEM characterizations indicate that the grains were oriented by hot-forging, and the c-axis is inclined to perpendicular to the pressing direction. Cantarero et al. [6] have proved that the carrier mobility in the c-axis direction is higher than that in the a-axis direction owing to the electron effective-mass anisotropy. The interplane parallel to the a–c or b–c plane provides a good path to electron transport, resulting in that the carrier mobility of $Bi_2S_{2.90}$ sample increases after hot-forging.

Fig. 3(c) shows the power factor as a function of measuring temperature for the Bi_2S_3's. The power factor for the Bi_2S_3 sample reaches 91 μW/mK^2 at 573 K and is about a half of that (181 μW/mK^2) for the $Bi_2S_{2.90}$ sample. The power factor for $Bi_2S_{2.90}$ sample further increases after hot-forging, and reaches the highest values 254 μW/mK^2 at 323 K for $Bi_2S_{2.90}$-T sample. This result means that power factor can be enhanced by optimizing carrier concentration and mobility through controlling sulfur contents and grain orientation.

Fig. 4(a) shows the thermal conductivity as a function of measuring temperature for the Bi_2S_3's. The thermal conductivities

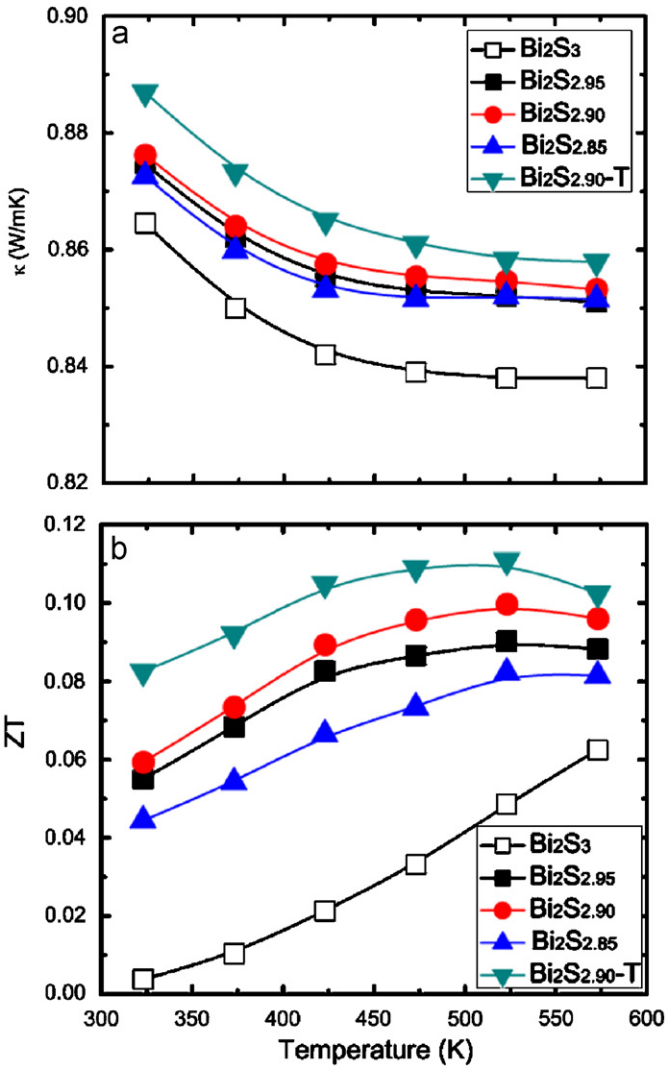

Fig. 4. Temperature dependence of thermal conductivity (a) and ZT (b) for Bi_2S_3's.

for all the samples show the same decreasing trend with increasing temperature. The thermal conductivity of Bi_2S_3 sample is the lowest, which ranges from 0.83 to 0.85 W/mK in the whole measuring temperature range. The total thermal conductivity is the sum of electronic and lattice contributions. Using the measured electrical resistivity in conjunction with the Wiedemann–Franz law, we estimate that the maximum thermal conductivity contributed from the electron is possible to be below 0.4% of the total thermal conductivity for Bi_2S_3 sample. It is well known that the decreased electrical resistivity will results in the increase of electronic thermal conductivity. The increased thermal conductivities for the Bi_2S_{3-x} ($x>0$) samples may be ascribed to

the decrease in electrical resistivity. The variations of thermal conductivity for the Bi_2S_{3-x} ($x>0$) samples show the reverse trend to that of electrical resistivity, that is, the thermal conductivity increases by decreasing sulfur contents to $x=2.90$ and then decreases by further decreasing sulfur to $x=2.85$. However, the thermal conductivity increases slightly since the contribution of the electronic thermal conductivity does not exceed 1–2% for the Bi_2S_{3-x} ($x>0$) samples. This means that the total thermal conductivity for Bi_2S_3's is approximately equal to the lattice thermal conductivity. In other words, the heat in Bi_2S_3's is mainly carried by lattice phonons. Compared with the lattice thermal conductivity at room temperature for the optimized *n*-type $Bi_2(Se,Te)_3$ polycrystalline materials (0.7 W/mK) [15], we note that the total thermal conductivity of Bi_2S_3's is well comparable to this value. The surprising low thermal conductivity of the Bi_2S_3 polycrystals may be attributed to the large numbers of weak ionic and van der Waals forces chemical bonds [12]. In addition, the present Bi_2S_3 polycrystals fabricated by MA and SPS have fine grain sizes, in which a large amount of grain boundaries also contribute to the reduced thermal conductivity. Hence, at least from the perspective of thermal transport, Bi_2S_3's satisfy one of the key requirements for a useful TE material, they possess very low thermal conductivity.

Fig. 4(b) shows the dimensionless figure of merit, ZT, as a function of measuring temperature for the Bi_2S_3's. The maximum ZT value at 573 K is 0.06 for the Bi_2S_3 sample that is the same to that of Bi_2S_3 synthesized by vacuum-melting [8]. However, the ZT value of Bi_2S_3's was double increased by producing sulfur vacancies and controlling the grain orientation. The enhanced ZT value was mainly ascribed to the significantly increased electrical transport properties and slightly increased thermal conductivity since the contribution of the electronic thermal conductivity was very weak. The ZT value reaches 0.09 at 523 K for the $Bi_2S_{2.90}$ sample, and further increases to 0.11 at 523 K for the hot-forged $Bi_2S_{2.90}$-T sample. The ZT value of 0.11 for Bi_2S_3's TE materials is the maximum reported so far.

4. Conclusions

Finally, Bi_2S_3 polycrystals were synthesized by a simple process combined mechanical alloying (MA) with spark plasma sintering (SPS) technique. The electrical resistivity was significantly reduced by modification of sulfur contents through producing the sulfur vacancies, and was further reduced by increasing the carrier mobility through forming oriented microstructure, whereby the power factor was significantly enhanced by modifying sulfur contents from 91 $\mu W/mK^2$ for Bi_2S_3 to 181 $\mu W/mK^2$ for $Bi_2S_{2.90}$, and further increased to 254 $\mu W/mK^2$ for the textured $Bi_2S_{2.90}$ by hot-forging. The thermal conductivity of Bi_2S_3's ranging from 0.83 to 0.89 W/mK, which is well comparable to or even lower than that of Bi_2Te_3 compounds. An enhanced maximum ZT value 0.11 at 523 K achieved for the textured $Bi_2S_{2.90}$ sample, which is the highest value known presently in the Bi_2S_3 system. Further enhancing electrical transport properties could be accomplished by optimizing the carrier concentrations and mobilities through controlling accurately the stoichiometry and grain orientation.

Acknowledgments

This work was conducted in Tsinghua University and supported by National Basic Research Program of China (Grant nos. 2007CB607504 and 2007CB607505).

References

[1] D.M. Rowe, Thermoelectrics Handbook: Macro to Nano, CRC Press, Boca Raton, 2006.
[2] M. Stordeur, in: D.M. Rowe (Ed.), CRC Handbook of Thermoelectrics, CRC Press, Boca Raton, 1995, p. 239.
[3] X.F. Tang, W.J. Xie, H. Li, W.Y. Zhao, Q.J. Zhang, M. Niino, Appl. Phys. Lett. 90 (2007) 012102-1–012102-3.
[4] K.F. Hsu, S. Loo, F. Guo, W. Chen, J.S. Dyck, C. Uher, T. Hogan, E.K. Polychroniadis, M.G. Kanatzidis, Science 303 (2004) 818–821.
[5] M. Zhou, J.-F. Li, T. Kita, J. Am. Chem. Soc. 130 (2008) 4527–4532.
[6] P. Cantarero, J. Martinez-Pastor, A. Segura, Phys. Rev. B 35 (1987) 9586–9590.
[7] H. Mizoguchi, H. Hosono, N. Ueda, H. Kawazoe, J. Appl. Phys. 78 (1995) 1376–1378.
[8] B. Chen, C. Uher, L. Iordanidis, M.G. Kanatzidis, Chem. Mater. 9 (1997) 1655–1658.
[9] S.-C. Liufu, L.-D. Chen, Q. Yao, C.-F. Wang, Appl. Phys. Lett. 90 (2007) 112106-1–112106-3.
[10] L.-D. Zhao, B.-P. Zhang, J.-F. Li, H.-L. Zhang, W.-S. Liu, Solid State Sci. 10 (2008) 651–658.
[11] A. Calka, A. Mosbah, N. Stanford, P. Balaz, J. Alloys Compd. 455 (2008) 285–288.
[12] J. Grigas, E. Talik, V. Lazauskas, Phys. Status Solidi B 232 (2002) 220–230.
[13] A.M. Ioffe, Semiconductor Thermoelements and Thermoelectric Cooling, Infosearch Ltd., Press, London, 1957.
[14] R.W.G. Wyckoff, Crystal Structure, Wiley, New York, 1964.
[15] L.D. Chen, Mater. Integration 18 (2005) 18–25.